# Local order and dynamic properties of liquid and undercooled $Cu_xZr_{1-x}$ alloys by *ab initio* molecular dynamics

N. Jakse[1] and A. Pasturel[1,2]

[1]*Sciences et Ingénierie des Matériaux et Procédés, INP Grenoble, UJF-CNRS, 1130 rue de la Piscine, BP 75, 38402 Saint-Martin d'Hères Cedex, France*

[2]*Laboratoire de Physique et Modélisation des Milieux Condensés, Maison des Magistères, BP 166 CNRS, 38042 Grenoble Cedex 09, France*

(Received 2 October 2008; revised manuscript received 14 November 2008; published 16 December 2008)

We report the results of first-principles molecular-dynamics simulations for liquid and undercooled $Cu_xZr_{1-x}$ alloys at four different compositions. The local structure as defined by the partial pair-correlation functions and the Bhatia-Thornton partial structure factors is found to display a strong evolution as a function of composition. In addition, a structural analysis using three-dimensional pair-analysis techniques evidences an icosahedral short-range order much more pronounced around $x_{Cu}=0.64$. In examining the dynamic properties of these alloys, we show a strong interplay between the structural changes and the evolution of the viscosity as a function of composition.

DOI: 10.1103/PhysRevB.78.214204 PACS number(s): 61.20.Ja, 61.25.Mv, 66.20.Cy

## I. INTRODUCTION

Since the discovery of glassy systems based on multicomponent alloys in the early 1990s,[1,2] bulk metallic glasses (BMGs) have been extensively studied because certain properties such as mechanical ones can be significantly improved over their crystalline counterparts. In order to make the best use of this new category of advanced materials, the key problem is to develop BMGs with superior glass-forming abilities (GFAs) with critical cooling rates often less than 10 K/s, giving the possibility to increase the critical casting thickness. Such desired characteristics may be related to a high thermal stability of the undercooled liquid state of these alloys and a great deal of efforts has been devoted to predict the element selection and compositional range of glass-forming alloys to stabilize the undercooled liquid state. For instance, Inoue[3] proposed three criteria for the stabilized undercooled liquid: (i) multicomponent systems consisting of more than three constituents, (ii) more than 12% atomic radius difference between constituents, and (iii) negative heats of mixing between the main constituent atoms. Although, these rules have played an important role as a guideline for the synthesis of BMGs, recent experimental measurements[4–6] have shown that binary Cu-Zr alloys can be also vitrified in BMGs. Moreover, it has been found that the GFA of Cu-Zr binary alloys displays a strong dependence as a function of compositions; the best glass former in this system, i.e., $Cu_{64.5}Zr_{35.5}$, is off eutectic.

While the understanding of the mechanisms of glass formation still remains a challenge at the present time, a comprehensive analysis of thermodynamic, structural, and kinetic properties is needed, especially in the undercooled region where the nucleation and growth or the glass transition take place. To explain the unusual stability of a system in the undercooled region, Frank[7] hypothesized that the local structures of undercooled melts of pure elements contain a significant degree of icosahedral short-range order (ISRO) incompatible with long-range periodicity. Very recently, such an assumption has been assessed for Ni, Zr, and Ti from x-ray scattering and neutron-diffraction experiments combined with electromagnetic[8] and electrostatic[9] levitation techniques, and has been also partially supported by *ab initio* molecular-dynamics (AIMD) simulations.[10] It has been shown that an ISRO already exists in the stable liquid but local configurations are more complex than the simple icosahedron. Moreover, this complexity has been found to depend on the system investigated and to increase in the undercooled region.[10] For instance, in zirconium, an increasing degree of bcc-type ordering upon undercooling occurs, in relation to the structure of the high-temperature solid phase. For liquid alloys, the occurrence of ISRO may become more questionable since alloying effects may enhance or disfavor ISRO. Within this framework, the element selection and compositional range of glass-forming alloys have been often thought to be relevant criteria to maximize ISRO in the liquid phase of such alloys, although direct experimental evidences for their importance were not made. It is also believed that ISRO may influence the dynamic properties of undercooled liquids. According to the scenario of Tanaka,[11] there is a close link between the local structure and kinetic aspects. A direct correlation between ISRO and the viscosity of the melt has been theoretically analyzed, and alloys having a stronger tendency to display an ISRO in the liquid might be less fragile, as characterized by the steepness of the viscosity-temperature profile, and therefore, should be better glass formers.

To study the interplay between the short-range structure of metallic liquid alloys and their GFA, an alternative is to perform simulations at the atomic level based on first-principles electronic structure calculations to capture the exact nature of SRO in such liquid alloys and to have an accurate description of its evolution in the undercooled region. Very recently, we investigated the structural properties of $Cu_{64}Zr_{36}$ alloy above and below its experimental liquidus temperature using AIMD simulations coupled to a structural analysis based on three-dimensional pair-analysis technique.[12] We have also studied the evolution of its viscosity as a function of the temperature, using a Vogel-Fulcher-Tammann (VTF) law. Our findings showed that $Cu_{64}Zr_{36}$ al-

 

loy, which is known to correspond to the best glass-forming composition in the binary Cu-Zr system, is characterized by a pronounced ISRO in the liquid, undercooled and amorphous states associated to the existence of $Cu_7Zr_6$ and $Zr_6Cu_{10}$ clusters centered by Cu and Zr atoms, respectively. Moreover we have found that the fragility lies in the same range than some ternary bulk-metallic-glass formers.[13] Given that the structural and dynamic properties of the Cu-Zr system in the liquid and undercooled states can be successfully described using AIMD simulations, in this paper, we address the important question of the evolution of the local structure as a function of composition by performing a series of simulations for $x_{Cu}=0.28$, 0.46, 0.64, and 0.80. Our AIMD results show a significant evolution of the local structure as a function of composition. By refining our study of the structural properties with the common-neighbor three-dimensional analysis,[14] our findings further indicate the maximum of ISRO around $x_{Cu}=0.64$ in agreement with the experimental glass-forming range. A dynamical image is proposed by analyzing the viscosity for all the studied compositions using a direct method based on a description of the collective dynamic properties by means of the transverse current-current correlation functions, and we show that the viscosity displays a maximum around $x_{Cu}=0.64$. Finally, in the Cu-rich side for which ISRO is the most important, we discuss the fragility parameter of liquid $Cu_xZr_{1-x}$ alloys with respect to those found in the best bulk-metallic-glass-forming alloys.

## II. COMPUTATIONAL DETAILS

### A. First-principles calculations

Our first-principles calculations are based on density-functional theory using the form of generalized gradient approximation developed by Perdew and Wang.[15] We use the most recent version of the Vienna *ab initio* simulation package[16] (VASP) in which the interactions between the ions and electrons are described by the projector augmented-wave (PAW) method.[17] The valence state of each element has been previously defined in the provided PAW potentials and the plane-wave cutoff is 274 eV.

### B. Molecular dynamics and inherent structures

All the dynamical simulations were carried out in the canonical ensemble (NVT) by means of a Nosé thermostat to control temperature. Newton's equations of motion were integrated using the Verlet algorithm with a time step of 3 fs. We have considered a system of 256 atoms in a cubic box with periodic boundary conditions. Only the $\Gamma$-point sampling was considered to sample the supercell Brillouin zone. To study the composition dependence of the local structure of liquid $Cu_xZr_{1-x}$ alloys, we have performed four molecular-dynamics (MD) simulations for compositions $x_{Cu}=0.28$, 0.46, 0.64, and 0.80 at temperature $T=1500$ K located above the liquidus lines. For Zr-rich compositions, the initial configuration was taken from a well-equilibrated liquid Zr system[10] in which random substitution of some Zr atoms with Cu atoms was done. We started from a liquid Cu configuration for Cu-rich compositions, and for $x_{Cu}=0.46$, we have checked that replacing Cu atoms by Zr atoms or vice versa gives the same results. For each composition, the volume of the cell has been fixed to reproduce the experimental densities.[18] It is worth mentioning that it results in lengths of the simulation boxes $L=16.978$, 16.360, 15.702, and 15.177 Å, respectively, for $x_{Cu}=0.28$, 0.46, 0.64, and 0.80, and that these finite-size effects have been examined in a previous study.[10] Each alloy is equilibrated at $T=1500$ K for 3 ps; the run was continued for 30 ps to perform the dynamic and structural analyses. Then, each alloy was quenched in the undercooled region and the same protocol than in the liquid state was used. At each composition, the undercooled state is defined by a temperature lower by 50 K than the experimental liquidus temperature.[19] Such a definition leads only to a small variation in temperature as a function of composition due to the peculiar shape of the Cu-Zr phase diagram. As the evolution of experimental densities in the undercooled region is unknown, we employed the same density for both liquid and undercooled alloys. For each composition and temperature, 2000 configurations were used to produce averaged structural quantities such as the partial pair-correlation functions. Among these configurations, ten selected ones regularly spaced in time are saved to extract their inherent structures.[20] To this end, the steepest-descent energy-minimization procedure with the conjugate gradient method is imposed on each of these configurations. This method allows us to uncouple the vibrational motion from the underlying structural properties since atoms are brought to a local minimum in the potential-energy surface. At $x=0.64$, the simulation done in the present work is an extension of the one made in a previous study.[12]

### C. Common-neighbor analysis

The inherent structures are used to perform a common-neighbor analysis (CNA) (Ref. 14) that is able to give a detailed three-dimensional image of the topology surrounding each atom. This method is able to distinguish between various local structures such as fcc, hcp, bcc, and icosahedral, as well as more complex polytetrahedral environments. Technically, the first two peaks of the pair-correlation function are decomposed, and the CNA is able to characterize the local environment surrounding each atomic pair that contributes to the peaks of $g(r)$, in terms of the number and properties of common nearest neighbors of the pair under consideration. Each bonded pair of atoms is classified according to the number and topology of the common neighbors using a set of four indices: (i) the first index denotes to what peak of $g(r)$ belongs the pair under consideration, i.e., the root pair 1 for the first peak and 2 for second peak of $g(r)$. (ii) The second index represents the number of near neighbors shared by the root pair. (iii) The third index is for the number of nearest-neighbor bonds among the shared neighbors. (iv) A fourth index is used to distinguish configurations with the same first three indices but with a different topology. The CNA can distinguish between the fcc, hcp, bcc, and icosahedral packing (see Ref. 10 for more details). For instance, 1421 and 1422 bonded pairs are characteristic of close-packed structures (fcc and hcp) while 1441 and 1661 are

typical pairs of the bcc crystal. On the other hand, the number of 1551 and 1541 bonded pairs is a direct measure of the degree of icosahedral ordering.

### D. Dynamic properties

In the present work, we have determined the viscosity using a direct method based on the collective dynamic properties through the transverse current-current correlation functions $C_T(q,t)$.[21] It has the advantage of yielding a generalized $q$-dependent viscosity from which the hydrodynamic limit can be evaluated. The function

$$C_T(q,t) = \frac{1}{N}\langle J_T^*(q,t) J_T(q,t)\rangle, \tag{1}$$

is defined in terms of $J_T(q,t)$, the transverse current that can be written along the $x$ direction as

$$J_T(q,t) = \sum_{j=1}^{N} v_{j,x}(t)\exp[iqz_j(t)]. \tag{2}$$

$v_{i,x}(t)$ is the $x$ component of the velocity of atom $i$ and $q$ is a wave vector along the $z$ direction. Two formally identical expressions can be written for $y$ and $z$ directions. The transverse current given by Eq. (3) has been extracted directly from the successive configurations in our AIMD simulations. All the functions $C_T(q,t)$ decay sufficiently fast to zero such as $\eta(q)$ can be obtained down to the smallest values of $q$ compatible with the size of the cubic simulation cell. The Fourier transform of $C_T(q,t)$ shows a well-defined peak whose position corresponds to shear mode frequencies, while its zero-limit Laplace transform $\tilde{C}_T(q,z=0)$ leads to the $q$-dependent shear viscosity

$$\eta(q) = \frac{\rho k_B T}{m_A q^2 \tilde{C}_T(q,z=0)}. \tag{3}$$

$m_A$ stands for the average mass of the atoms and $\rho$ is the number density. The shear viscosity $\eta$ can be inferred by extrapolating $\eta(q)$ to $q=0$. This is done by fitting $\eta(q)$ with the function

$$\eta(q) = \frac{\eta}{1 + a^2 q^2}, \tag{4}$$

which was used first by Alley and Alder[22] to represent the viscosity of a dense hard-sphere packing.

## III. RESULTS AND DISCUSSION

### A. Structural properties of pure elements

We analyzed first the results of AIMD simulations for pure Zr and Cu in the liquid and undercooled states. For Zr, the results have been already published previously.[10] In this paper, we report only the main findings obtained in the liquid regime at $T=2500$ K and in the undercooled state at $T=2000$ K (the experimental melting temperature is 2123 K) because they will be used in comparison with results obtained for Cu and $Cu_xZr_{1-x}$ alloys. For Cu, two temperatures are considered, namely, $T=1623$ and 1313 K and the volume of simulation cells has been fixed to reproduce the experimental densities.[23] The first temperature is in the stable liquid, above the experimental melting temperature of 1356 K, while the second one is in the undercooled regime.

TABLE I. Coordination numbers $z^1$ and analysis in bonded pairs for Zr in the liquid ($T=2500$ K) and undercooled ($T=2000$ K) states, as well as for Cu in the liquid ($T=1623$ K) and undercooled ($T=1313$ K) states. The absolute error bars of the abundances of the pairs are 0.01.

| | Zr | | Cu | |
|---|---|---|---|---|
| $T$ (K) | 2500 | 2000 | 1623 | 1313 |
| $z^1$ | $13.2 \pm 02$ | $13.9 \pm 02$ | $12.2 \pm 02$ | $12.6 \pm 02$ |
| 15$xx$ | 0.48 | 0.37 | 0.47 | 0.48 |
| 142$x$ | 0.02 | 0.01 | 0.11 | 0.11 |
| 1441 | 0.10 | 0.14 | 0.07 | 0.05 |
| 1661 | 0.16 | 0.23 | 0.10 | 0.07 |

The coordination numbers, which have been determined from the calculated pair-correlation functions $g(r)$,[10] give the first indication of the nature of SRO. In the liquid state, the coordination number found for Cu is significantly smaller than that of Zr as shown in Table I. For both elements, an increase in the coordination number is found upon undercooling. For Zr, this is also observed experimentally, although the calculated values are slightly higher than the experimental ones.[10] For Cu, the evolution of the coordination number is less important due in part to a smaller range of temperature. As already reported by Ganesh and Widom,[23] it is not possible to achieve a higher degree of undercooling of Cu because a partial crystallization of samples occurs at lower temperatures than 1313 K. In the liquid or undercooled region, a value for the coordination number higher than 12 implies that the coordination polyhedron surrounding each atom is larger than the simple icosahedron on average. This is illustrated in Fig. 1, where the distribution of their different sizes is drawn for both elements. A non-negligible part of the clusters are Frank-Kasper (FK) polyhedra of high coordination, namely, Z13, Z14, and even Z15 for Zr atoms, showing that the SRO is more complex than that based on the simple icosahedron (Z12). Let us mention that this complexity appears to be more important for Zr than for Cu.

A more detailed image of the topology of the polyhedra surrounding Cu and Zr atoms is obtained from the common-neighbor analysis performed on ten inherent structures. The resulting average abundance of pairs is reported in Table I. For both elements, it is seen that the fivefold symmetry dominates in the stable liquid state since the abundance of 15$xx$ pairs that correspond to the sum of 1551 and 1541 pairs is the largest. Moreover, this analysis confirms that the local environment of Zr atoms is quite different from that of Cu atoms, as already observed from their coordination number. More particularly, for Zr atoms, the 1661 and 1441 bonded pairs are more important, supporting the occurrence of an increasing complexity of the Frank-Kasper based polytetrahedral symmetry around these atoms. On the other hand, the non-negligible number of 142$x$ pairs (sum of 1422 and 1421

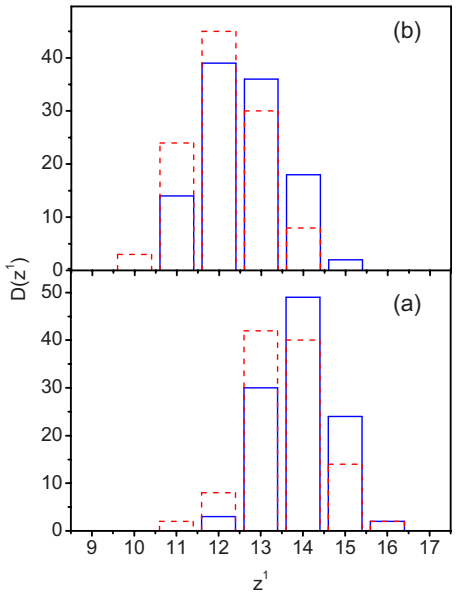


FIG. 1. (Color online) Distribution of the coordination numbers $z^1$ for typical configurations in the liquid (dashed lines) and undercooled states (solid lines) for (a) Zr and (b) Cu.

pairs) for Cu atoms is in favor of the close-packed structures. The way in which SRO evolves upon undercooling is different for Zr and Cu atoms even if the fivefold symmetry remains always the most important feature. Undercooled liquid copper shows a weak increase in icosahedral symmetry in agreement with recent experiments[24] and the *ab initio* study of Ganesh and Widom.[23] For Zr, the situation is quite different. Upon undercooling, the number of 15*xx* bonded pairs decreases while the number of 1441 and 1661 pairs increases. Thus these two variations favor a growing degree of a bcc-type structure, as well as an increasing complexity of the Frank-Kasper-based polytetrahedral symmetry.

Then to conclude this first part, Cu and Zr liquids display ISRO but with two different local environments and also with a different evolution upon undercooling. These results raise an important question: do alloying effects in the binary Cu-Zr system offer the possibility to optimize icosahedral order? Indeed, alloying effects lead to chemical short-range order (CSRO) but such effect may enhance or disfavor ISRO. In Sec. II B, we present the evolution of ISRO as a function of composition in the binary Cu-Zr system.

### B. Structural properties of $Cu_xZr_{1-x}$ alloys

In order to analyze the evolution of SRO in the binary Cu-Zr system, we have calculated several structural quantities in order to emphasize their evolution as a function of composition and also as a function of temperature. Namely, for the four alloys $Cu_xZr_{1-x}$ with $x=0.28$, 0.46, 0.64, and 0.80, we have considered the partial pair-correlation functions $g_{ij}(r)$ as shown in Figs. 2 and 3 for liquid and undercooled states, respectively. They are important quantities to characterize local structures of liquid alloys since $g_{ij}(r)$ is defined to be the number of $j$ atoms found at a distance $r$ from an $i$ atom. We have determined the nearest-neighbor

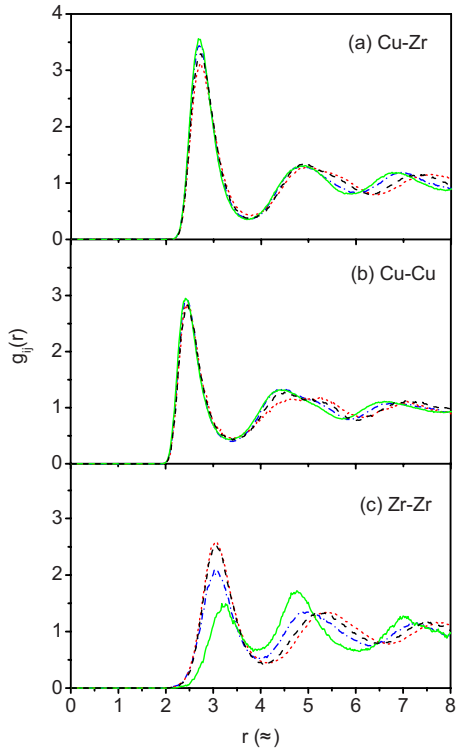


FIG. 2. (Color online) Partial pair-correlation functions of $Cu_x$-$Zr_{1-x}$ in the liquid state ($T=1500$ K) for $x_{Cu}=0.28$ (dotted lines), $x_{Cu}=0.46$ (dashed lines), $x_{Cu}=0.64$ (dash-dotted lines), and $x_{Cu}=0.80$ (solid lines): (a) Cu-Zr, (b) Cu-Cu, and (c) Zr-Zr.

coordination number $z^1_{CuCu}$, $z^1_{CuZr}$, and $z^1_{ZrZr}$ by counting the number of atoms in the first coordination shells directly from the configurations, which is equivalent to integrating the radial distribution functions $RDF_{ij}(r)=c_j 4\pi\rho r^2 g_{ij}(r)$ ($\rho$ being the atomic density) up to the first minimum of $g_{ij}(r)$. The partial nearest-neighbor distances, $r_{CuCu}$, $r_{CuZr}$, and $r_{ZrZr}$, have been estimated from the first maxima of the $g_{ij}(r)$'s.[10] All these values are gathered in Table II, while the evolution of the total coordination number as well as the coordination number around each species is shown in Fig. 4.

As a first step, we discuss the evolution of the partial pair-correlation functions as a function of composition. The partial pair-correlations between Cu and Zr, $g_{CuZr}(r)$, at the four compositions are shown in Fig. 2(a). The height of the first peak in $g_{CuZr}(r)$ increases when the Cu concentration $x$ increases from 0.2 to 0.8 while its position is virtually unchanged. This first result suggests that Cu and Zr atoms are well mixed in the liquid phase. The partial pair-correlation functions between Cu atoms, $g_{CuCu}(r)$, are shown in Fig. 2(b). The height of the first peak increases only slightly with increasing the concentration of Cu and its position is not sensitive to the Cu concentration. The situation is quite different for the Zr-Zr interaction since the height of the principal peak of the partial pair-correlation function between the Zr atoms displays an important decrease with increasing the composition of Cu as shown in Fig. 2(c). In the same time, the increase in the second peak is another striking feature. The positions of both peaks are also very sensitive to the Cu composition; the first peak shifts toward the largest value

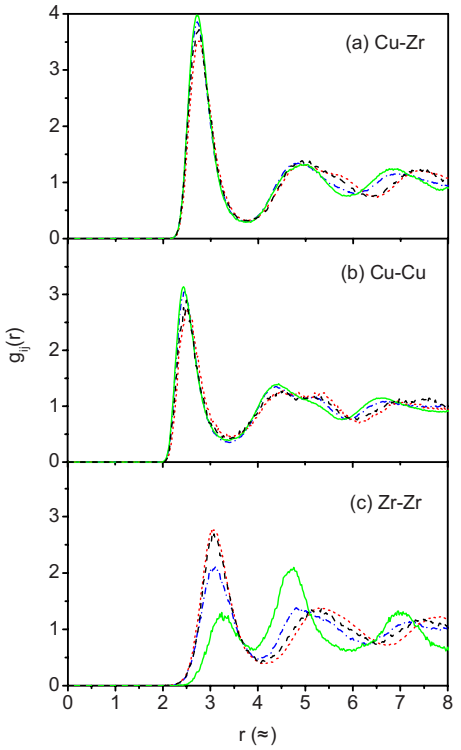


FIG. 3. (Color online) Partial pair-correlation functions of $Cu_x$-$Zr_{1-x}$ in the undercooled state. Same caption as in Fig. 2.

from 3.06 to 3.24 Å while the second peak shifts toward the smaller values. Then Zr-Zr interactions play an important role in the evolution of the local structure of liquid $Cu_xZr_{1-x}$ alloys as a function of composition. Let us mention that our theoretical results do not support the assumption used in the experimental work of Ref. 25 that the partial functions $g_{ij}(r)$ do not change with composition.

In Fig. 3, we present the partial pair-correlation functions $g_{ij}(r)$ of the undercooled state. Upon undercooling, changes are very small for all compositions, with only a weak increase in the first peak height and an enhancement of a shoulder of the second peak of the three partials. This leads us to the conclusion that the undercooled state is characterized by a local arrangement similar to that of the liquid state.

The Bhatia-Thornton partial structure factors provide also valuable information regarding short-range order (SRO) in binary liquid alloys. In Fig. 5, we present the calculated factors $S_{NN}(q)$, $S_{cc}(q)$, and $S_{Nc}(q)$ for the four compositions of the liquid state. Let us mention that like for the partial pair-correlation functions, changes in Bhatia-Thornton partial structure factors are very small upon undercooling. The density-density factor, $S_{NN}(q)$, describes the topological properties of the spatial arrangement of the means atoms, i.e., the topological short-range order (TSRO) of system, while the concentration-concentration factor, $S_{cc}(q)$, describes the local fluctuations in the concentration, and hence, its CSRO. The cross term, $S_{Nc}(q)$, which couples the density and concentration variables, is related to the size difference between both alloying species.

First, we discuss the evolution of TSRO as a function of composition through the calculated $S_{NN}(q)$ shown in Fig. 5(a). A number of features deserve mention: (i) the variation in the positions of the two main peaks as a function of composition is related to the evolution of the atomic density. (ii) No significant change in the shape of these peaks is observed. For all the compositions, we note that the second peak exhibits a shoulder on the right-hand side, leading to a rather asymmetrical shape extending from $1.7q_1$ to $2q_1$, $q_1$ is the position of the first peak. Despite the absence of a clear second-peak splitting which is suggestive of local icosahedral order,[26] we can note that the height ratio between the first peak and the second peak is equal to 0.49, similar to the theoretical value obtained by using a Landau description of short-range icosahedral order.[26] In Fig. 5(b), the very small amplitudes of oscillations of $S_{Nc}(q)$ indicate that the atomic sizes of Cu and Zr are not very different in liquid $Cu_xZr_{1-x}$ alloys.

For the four compositions, the calculated functions $S_{cc}(q)$ reproduce a peak centered around 1.9 $Å^{-1}$, which is indicative of a chemical SRO in liquid $Cu_xZr_{1-x}$ alloys [see Fig. 5(c)]. This results from a chemical order between Cu and Zr atoms, and we note that the peak becomes more pronounced with increasing the Cu composition. As discussed above, this evolution can be related to the peculiar evolution of Zr-Zr interactions as a function of composition.

TABLE II. Partial nearest-neighbor distances $r_{ij}$, partial first-neighbor coordination numbers $z_{ij}^1$, generalized chemical short-range order parameter $\alpha_1$ together with its normalized value $\alpha_1^0$, and the self-diffusion coefficient $D$ for $Cu_x$-$Zr_{1-x}$ for the different copper concentrations $x_{Cu}$ in the liquid state ($T$=1500 K) and in the undercooled region.

| $x_{Cu}$ | 0.28 | 0.46 | 0.64 | 0.80 |
|---|---|---|---|---|
| | | Liquid | | |
| $z_{Cu\text{-}Cu}^1$ | 2.3 | 4.2 | 6.5 | 8.9 |
| $z_{Zr\text{-}Zr}^1$ | 10.3 | 7.9 | 5.2 | 2.4 |
| $z_{Cu\text{-}Zr}^1$ | 8.8 | 7.4 | 5.6 | 3.5 |
| $r_{Cu\text{-}Cu}$ | 2.46 | 2.44 | 2.42 | 2.42 |
| $r_{Cu\text{-}Zr}$ | 2.72 | 2.70 | 2.72 | 2.70 |
| $r_{Zr\text{-}Zr}$ | 3.04 | 3.06 | 3.06 | 3.14 |
| $\alpha_1$ | −0.032 | −0.070 | −0.104 | −0.120 |
| $\alpha_1^0$ | 0.11 | 0.11 | 0.15 | 0.38 |
| $D$ ($Å^2$/ps) | 0.12 | 0.10 | 0.05 | 0.08 |
| | | Undercooled | | |
| $z_{Cu\text{-}Cu}^1$ | 2.3 | 4.1 | 6.4 | 8.9 |
| $z_{Zr\text{-}Zr}^1$ | 10.4 | 8.0 | 5.2 | 2.3 |
| $z_{Cu\text{-}Zr}^1$ | 8.9 | 7.4 | 5.6 | 3.5 |
| $r_{Cu\text{-}Cu}$ | 2.52 | 2.50 | 2.46 | 2.44 |
| $r_{Cu\text{-}Zr}$ | 2.74 | 2.74 | 2.72 | 2.70 |
| $r_{Zr\text{-}Zr}$ | 3.08 | 3.08 | 3.08 | 3.26 |
| $\alpha_1$ | −0.033 | −0.072 | −0.106 | −0.13 |
| $\alpha_1^0$ | 0.11 | 0.11 | 0.15 | 0.40 |
| $D$ ($Å^2$/ps) | 0.021 | 0.019 | 0.018 | 0.020 |

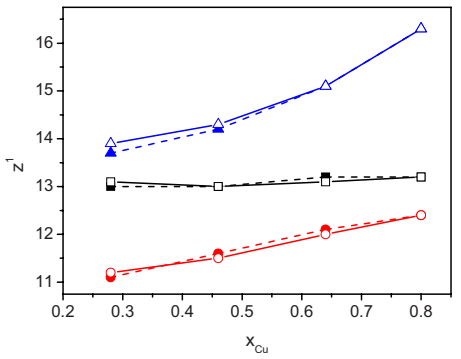


FIG. 4. (Color online) Evolution of the coordination numbers as a function of copper concentration $x_{Cu}$. The full symbols and the dashed lines correspond to the liquid state ($T$=1500 K), while the open symbols and the solid lines are for the undercooled state. Squares: total coordination numbers; circles: coordination number around Cu; triangles: coordination number around Zr.

To obtain a more quantitative estimate for the CSRO and its dependence with temperature, we consider the Warren CSRO parameter $a_1$ generalized by Wagner and Ruppersberg[27] to systems with size effects. $\alpha_1$, and its normalized value $\alpha_1^0$ with respect to the maximum order parameter $\alpha_1^{\max}$, are calculated using the values of $z_{ij}^1$ of Fig. 4 as follows:

$$\alpha_1 = 1 - z_{ij}^1/c_j(c_i z_j^1 + c_j z_i^1), \tag{5}$$

with $z_i^1 = z_{ii}^1 + z_{ij}^1$ $(i,j = \mathrm{Cu}, \mathrm{Zr})$

$$\alpha_1^0 = \alpha_1/\alpha_1^{\max} \text{ and } \alpha_1^{\max} = 1 - z_i^1/c_j(c_i z_j^1 + c_j z_i^1), \tag{6}$$

where $c_j$ the concentration of $j$ species. The calculated values of $\alpha_1$ and $\alpha_1^0$ are compiled for both liquid and undercooled states in Table II. These values confirm that the CSRO is concentration dependent with a strong increase around $x_{Cu}$ =0.80 while its dependence on temperature is not significant.

More insight into the structural changes can be gained by making use of the common-neighbor analysis. Like for pure elements, such an analysis is performed on ten inherent structures from which an average abundance of pairs is determined. In Table III, we report the main bonded pairs as found in pure elements to discuss the composition dependence of the local structure in liquid and undercooled $Cu_xZr_{1-x}$ alloys. The microscopic analysis emerging from Table III indicates that the short-range order of the liquid and undercooled states of $Cu_xZr_{1-x}$ alloys is similar and dominated by icosahedral and distorted icosahedral short-range order, since the fivefold symmetry is preponderant for both Cu and Zr atoms in the whole range of composition. By comparison with data of pure elements (see Table I), the degree of ISRO based on the number of 15$xx$ pairs is found to be much more important than those of the pure Zr and Cu metallic melts taken separately, showing that alloying effects play an important role in increasing ISRO. We can also note that the contributions of 1441 and 142$x$ pairs related to the tetrahedral local order become less important in $Cu_xZr_{1-x}$ alloys than those found in pure Zr and Cu, respectively. At $x_{Cu}$=0.64, the degree of ISRO with 60% of pairs being 15$xx$ is found to be the highest with respect to other compositions. This maximum is lower than that found for CSRO, and therefore, we cannot attribute the increase in ISRO in $Cu_xZr_{1-x}$ alloys only to chemical effects. If the number of 15$xx$ pairs is similar for Cu and Zr atoms whatever the composition is, the presence of two different percentages of 1661 pairs around these atoms indicate that the local environment of Zr atoms is quite different from that of Cu atoms. More particularly for Zr atoms, the importance of 1661 bonded pairs supports the occurrence of an increasing complexity of the Frank-Kasper polytetrahedral symmetry around them. This complexity can be also found by inspecting the coordination numbers of Zr and Cu in Fig. 4. The coordination number of Zr is always higher than that of Cu and displays a stronger variation with respect to the composition since it varies from 13.9 for $x_{Cu}$=0.28 to 16.3 for $x_{Cu}$=0.80 while the coordination number of Cu changes from 11.2 to 12.4. Our results are in agreement with recent experimental contribution based on a combination of neutron diffraction and reverse Monte-Carlo (RMC) modeling[28] emphasizing two different atomic configurations around Cu and Zr atoms.

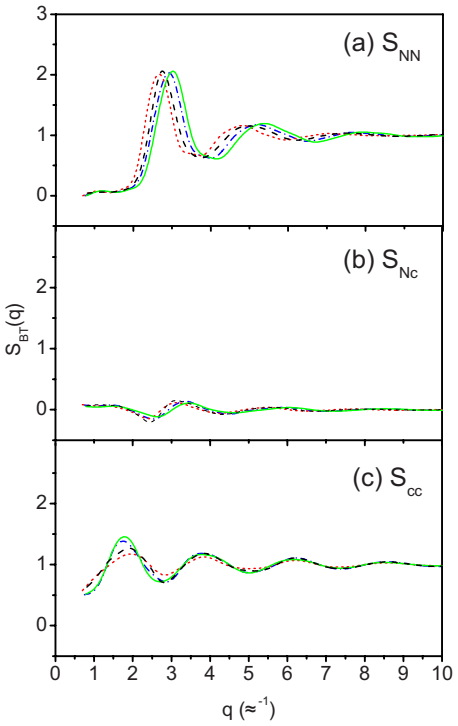


FIG. 5. (Color online) Bhatia-Thornton structure factors of $Cu_x$-$Zr_{1-x}$ in the liquid state ($T$=1500 K) for $x_{Cu}$=0.28 (dotted lines), $x_{Cu}$=0.46 (dashed lines), $x_{Cu}$=0.64 (dash-dotted lines), and $x_{Cu}$=0.80 (solid lines): (a) $S_{NN}(q)$, (b) $S_{Nc}(q)$, and (c) $S_{cc}(q)$.

Then we can conclude that the optimization of the icosahedral order in $Cu_xZr_{1-x}$ alloys is due to a subtle interplay between chemical and topological effects. As already discussed in Ref. 12, at $x_{Cu}$=0.64, this interplay leads to the occurrence of well-defined building units, namely, $Cu_7Zr_6$ and $Zr_6Cu_{10}$ clusters centered by Cu and Zr atoms, respectively.

TABLE III. Analysis in bonded pairs of $Cu_x$-$Zr_{1-x}$ for the different copper concentrations $x_{Cu}$ in the liquid state ($T=1500$ K) and in the undercooled region. The absolute error bars in the abundances are 0.01.

| | $x_{Cu}=0.28$ | | | | | |
|---|---|---|---|---|---|---|
| | Liquid | | | Undercooled | | |
| | Cu | Zr | Total | Cu | Zr | Total |
| 15*xx* | 0.55 | 0.52 | 0.53 | 0.55 | 0.52 | 0.53 |
| 142*x* | 0.05 | 0.04 | 0.04 | 0.04 | 0.04 | 0.04 |
| 1441 | 0.08 | 0.08 | 0.08 | 0.08 | 0.09 | 0.09 |
| 1661 | 0.06 | 0.17 | 0.14 | 0.06 | 0.17 | 0.14 |
| | $x_{Cu}=0.46$ | | | | | |
| | Liquid | | | Undercooled | | |
| | Cu | Zr | Total | Cu | Zr | Total |
| 15*xx* | 0.56 | 0.55 | 0.55 | 0.56 | 0.55 | 0.55 |
| 142*x* | 0.06 | 0.05 | 0.05 | 0.06 | 0.05 | 0.05 |
| 1441 | 0.08 | 0.07 | 0.08 | 0.08 | 0.08 | 0.08 |
| 1661 | 0.08 | 0.17 | 0.13 | 0.08 | 0.18 | 0.13 |
| | $x_{Cu}=0.64$ | | | | | |
| | Liquid | | | Undercooled | | |
| | Cu | Zr | Total | Cu | Zr | Total |
| 15*xx* | 0.61 | 0.58 | 0.60 | 0.60 | 0.58 | 0.59 |
| 142*x* | 0.04 | 0.04 | 0.04 | 0.04 | 0.04 | 0.04 |
| 1441 | 0.08 | 0.05 | 0.07 | 0.08 | 0.05 | 0.07 |
| 1661 | 0.12 | 0.19 | 0.14 | 0.12 | 0.18 | 0.14 |
| | $x_{Cu}=0.80$ | | | | | |
| | Liquid | | | Undercooled | | |
| | Cu | Zr | Total | Cu | Zr | Total |
| 15*xx* | 0.57 | 0.56 | 0.57 | 0.57 | 0.56 | 0.57 |
| 142*x* | 0.09 | 0.09 | 0.09 | 0.10 | 0.10 | 0.10 |
| 1441 | 0.06 | 0.03 | 0.05 | 0.06 | 0.03 | 0.05 |
| 1661 | 0.12 | 0.20 | 0.14 | 0.11 | 0.19 | 0.13 |

### C. Dynamic properties of $Cu_xZr_{1-x}$ alloys

To identify the effects of ISRO on the dynamic properties of stable and undercooled liquids, we have computed the viscosities from AIMD runs at $T=1500$ and 1200 K for the four alloys. Let us mention than $T=1200$ K is close to the different temperatures used to define the undercooled region as a function of composition. We report the evolution of the viscosity as a function of composition for both temperatures in Fig. 6. The experimental value of the viscosity at $T=1208$ K and at $x_{Cu}=0.50$ (Ref. 29) is also reported to visualize the quality of simulations. At $x_{Cu}=0.64$, we also estimated the viscosity as a function of temperature $T$ through the Stokes-Einstein (SE) relation $\eta_E=k_BT/2\pi RD$, $k_B$ being Boltzmann's constant and $R$ taken as the position of the total pair-correlation function. The self-diffusion coefficient $D$ has been determined from the long time slope of the mean-square displacement and has been found to be equal to 0.05 Å$^2$/ps at $T=1500$ K and 0.018 Å$^2$/ps $T=1200$ K (see Table II). The values $\eta_E=16.3$ and 57 mPa s obtained, respectively, at $T=1500$ and 1200 K can be compared to those obtained by the direct method, namely, $\eta=18.3$ and 164 mPa s. This comparison indicates that the SE relation gives rise to reasonable results in the liquid state, but breaks down as the temperature decreases. This also holds for the other concentrations. Therefore this relation cannot be used to study the evolution of the viscosity as a function of temperature.

The most salient result is that the viscosity presents a maximum value at $x_{Cu}=0.64$ for which the ISRO has been found to be the most important. The viscosity displays also a more important evolution as the function of temperature on the Cu-rich side. Then our results support the scenario of a direct correlation between ISRO and the viscosity.[11] How-

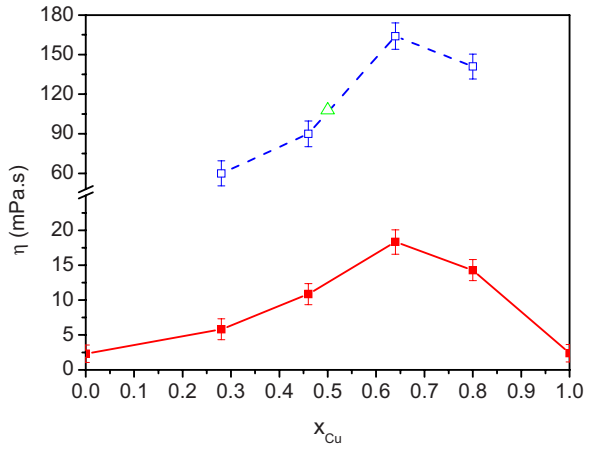


FIG. 6. (Color online) Evolution of the viscosity in the liquid state ($T=1500$ K, full symbols and solid lines) and at $T=1200$ K (open symbols and dashed lines) as a function of copper concentration $x_{Cu}$. The error bars on the calculated viscosities are also drawn, which amount to a relative error of always less than 8%. The open triangle corresponds to the experimental data of Ref. 29.

ever values obtained in the liquid Cu-Zr system are much lower than those found for the best bulk-metallic-glass-forming alloys. For instance the melt viscosities measured for the $Zr_{46.75}Ti_{8.25}Cu_{7.5}Ni_{10}Be_{27.5}$ and the $Zr_{41.2}Ti_{13.8}Cu_{12.5}Ni_{10}Be_{22.5}$ alloys are equal to 35 and 8 Pa s, respectively.[30] Such alloys are then about three orders of magnitude more viscous at the melting point than all liquid $Cu_xZr_{1-x}$ alloys. Such a difference is mainly due to the fact that even if ISRO is important in this alloy family, the degree of short-range ordering is not sufficient to favor a spatial connectivity between well-defined local entities and then the development of a stable medium-range structure.[31] Indeed, such a structural ordering would lead to a decrease in the configurational entropy of the liquid, and according to the Adams-Gibbs theory[32] this would result in a more viscous liquid.

To confirm this analysis, we calculate the fragility parameter for Cu-rich compositions for which ISRO and CSRO are the most important, and the calculated values of the viscosity are the largest. The viscosity of the molten liquid is associated with the liquid fragility, a concept introduced by Angell[33] to differentiate liquids with various dynamic characteristics. A strong liquid exhibits an Arrhenius-type temperature dependence of the viscosity, whereas the temperature dependence of the viscosity for a fragile liquid deviates from the Arrhenius behavior with a steep change in the viscosity at the glass transition $T_G$. The temperature evolution of the viscosity is most often represented by the empirical VTF (Ref. 33):

$$\eta(T) = \eta_0 \exp\left(\frac{BT_0}{T-T_0}\right), \tag{7}$$

where $B$ is constant and $T_0$ is a characteristic temperature for which the viscosity diverges. The high-temperature limit of the viscosity $\eta_0 = h/V_A$ can be readily calculated within the rate theory[34] from Planck's constant $h$ and atomic volume $V_A$. The temperature dependence of the viscosity is obtained from first principles as the following: we use the *ab initio* values given above as well as that of the experimental glass transition temperature[4,19] where the viscosity is chosen to be the conventional value $\eta = 10^{12}$ Pa s.[33] For Cu-rich compositions, namely, $x_{Cu}=0.64$ and 0.8, $B$ and $T_0$ are obtained by a fit of the VTF equation, giving the temperature dependence of the viscosity. Let us mention that $B$ and $T_0$ values are not sensitive to small differences found in the experimental determinations of $T_G$. From these plots, we can define the fragility parameter as

$$m = \left[\frac{d(\log\ \eta)}{d(T_G/T)}\right]_{T=T_G}, \tag{8}$$

and using Eq. (7) we have

$$m = BT_0T_G/[2.3(T_G - T_0)^2]. \tag{9}$$

The fragility parameter $m$ is found to be equal to 88 and 130 for $x_{Cu}=0.64$ and 0.80, respectively. They are much higher than those of the best bulk-metallic-glass-forming alloys that are around 20,[35] and such results confirm that the short-range ordering in the liquid $Cu_xZr_{1-x}$ alloys is not important enough to give strong glass formers. Such a "fragile" character would imply an increase in SRO near the glass transition and, therefore, a possible evolution of the local structure in the amorphous state. Such a study is beyond the scope of this contribution, but very recent classical MD simulations of $Cu_xZr_{1-x}$ alloys ($x=0.46$ to 0.64) (Ref. 36) evidence the development of icosahedral ordering near the glass transition around Cu atoms, this ordering being more pronounced around $x_{Cu}=0.64$.

## IV. CONCLUSION

We have presented a first-principles based study of liquid and undercooled $Cu_xZr_{1-x}$ alloys in order to analyze their local order as a function of composition. The determination of the partial pair-correlation functions and the Bhatia-Thornton partial structure factor $S_{cc}(q)$ gives evidence of an increase in chemical SRO on the Cu-rich side. Moreover, for all compositions, the calculations of partial coordination numbers and the common-neighbor analysis clearly show that the degree of the icosahedral local symmetry is much more important than those of the pure Zr and Cu metallic melts taken separately with a maximum occurring around $x_{Cu}=0.64$. However if the predominance of the fivefold symmetry is close to the icosahedral one, the local environment of Zr atoms displays a more complex Frank-Kasper-based polytetrahedral symmetry. We show an impact of ISRO on the dynamic properties since the viscosity displays also a maximum around $x_{Cu}=0.64$ and an evolution as a function of temperature much more important on the Cu-rich side. However, at the melting point, our results of the viscosity show that $Cu_xZr_{1-x}$ alloys are less viscous by about 3 orders of magnitude than the best bulk-metallic-glass-forming alloys. Such a different behavior is also confirmed from comparison

of the fragility since the calculated fragility parameters of Cu-rich $Cu_xZr_{1-x}$ alloys are in the range of 90–130, showing that these alloys remain fragile liquids. It is mainly due to the fact the degree of short-range ordering in liquid $Cu_xZr_{1-x}$ alloys is smaller than those of the bulk-metallic-glass formers.

**ACKNOWLEDGMENTS**

We acknowledge the CINES and IDRIS under Project No. INP2227/72914, as well as PHYNUM CIMENT for computational resources. The ANR is gratefully acknowledged for financial support under Grant No. ANR:BLAN06-3_138079.

[1] A. Inoue, T. Zhang, and T. Masumoto, Mater. Trans., JIM **31**, 425 (1990).
[2] A. Peker and W. L. Johnson, Appl. Phys. Lett. **63**, 2342 (1993).
[3] A. Inoue, Acta Mater. **48**, 279 (2000).
[4] D. H. Xu, B. Lohwongwatana, G. Duan, W. L. Jonhson, and C. Garland, Acta Mater. **52**, 2621 (2004).
[5] A. Inoue and W. Zhang, Mater. Trans. **45**, 584 (2004).
[6] D. Wang, Y. Li, B. B. Sun, M. L. Sui, K. Lu, and E. Ma, Appl. Phys. Lett. **84**, 4029 (2004).
[7] F. C. Frank, Proc. R. Soc. London, Ser. A **215**, 1022 (1950).
[8] T. Schenk, D. Holland-Moritz, V. Simonet, R. Bellissent, and D. M. Herlach, Phys. Rev. Lett. **89**, 075507 (2002).
[9] G. W. Lee, A. K. Gangopadhyay, K. F. Kelton, R. W. Hyers, T. J. Rathz, J. R. Rogers, and D. S. Robinson, Phys. Rev. Lett. **93**, 037802 (2004).
[10] N. Jakse and A. Pasturel, Phys. Rev. Lett. **91**, 195501 (2003); N. Jakse, O. Le Bacq, and A. Pasturel, Phys. Rev. B **70**, 174203 (2004); N. Jakse and A. Pasturel, J. Chem. Phys. **120**, 6124 (2004); Mod. Phys. Lett. B **20**, 655 (2006); Phase Transitions **80**, 369 (2007).
[11] H. Tanaka, J. Phys.: Condens. Matter **15**, L491 (2003).
[12] N. Jakse and A. Pasturel, Appl. Phys. Lett. **93**, 113104 (2008).
[13] S. C. Glade and W. L. Johnson, J. Appl. Phys. **87**, 7249 (2000).
[14] J. D. Honeycutt and H. C. Andersen, J. Phys. Chem. **91**, 4950 (1987).
[15] Y. Wang and J. P. Perdew, Phys. Rev. B **44**, 13298 (1991).
[16] G. Kresse and J. Furthmuller, Comput. Mater. Sci. **6**, 15 (1996).
[17] G. Kresse and D. Joubert, Phys. Rev. B **59**, 1758 (1999).
[18] W. L. Johnson and K. Samwer, Phys. Rev. Lett. **95**, 195501 (2005).
[19] T. Abe, M. Shimono, M. Ode, and H. Onodera, Acta Mater. **54**, 909 (2006).
[20] F. H. Stillinger and T. A. Weber, Phys. Rev. A **25**, 978 (1982).
[21] N. Jakse, J. F. Wax, and A. Pasturel, J. Chem. Phys. **126**, 234508 (2007).
[22] W. E. Alley and B. J. Alder, Phys. Rev. A **27**, 3158 (1983).
[23] P. Ganesh and M. Widom, Phys. Rev. B **74**, 134205 (2006).
[24] A. Di Cicco, A. Trapananti, S. Faggioni, and A. Filipponi, Phys. Rev. Lett. **91**, 135505 (2003).
[25] N. Mattern, U. Kühn, A. Concustell, A. Schöps, M. D. Baro, and J. Eckert, Mater. Trans. **48**, 1639 (2007).
[26] S. Sachdev and D. R. Nelson, Phys. Rev. Lett. **53**, 1947 (1984); Phys. Rev. B **32**, 4592 (1985).
[27] C. N. J. Wagner and H. Ruppersberg, At. Energy Rev. **1**, 101 (1981).
[28] T. Fukunaga, K. Itoh, T. Otomo, K. Mori, M. Sugiyama, H. Kato, M. Hasegawa, A. Hirata, Y. Hirotsu, and A. C. Hannon, Intermetallics **14**, 893 (2006).
[29] G. J. Fan, M. Freels, H. Choo, P. K. Liaw, J. J. Z. Li, Won-kyu Rhim, W. L. Johnson, P. Yu, and W. H. Wang, Appl. Phys. Lett. **89**, 241917 (2006).
[30] W. H. Wang, P. Wen, D. Q. Zhao, M. X. Pan, and R. J. Wang, J. Mater. Res. **18**, 2727 (2003).
[31] H. W. Sheng, H. Z. Liu, Y. Q. Cheng, J. Wen, P. L. Lee, W. K. Luo, S. D. Shastri, and E. Ma, Nature Mater. **6**, 192 (2007).
[32] G. Adam and J. H. Gibbs, J. Chem. Phys. **43**, 139 (1965).
[33] C. A. Angell, Science **267**, 1924 (1995); L. Battezzati and A. L. Greer, Acta Metall. **37**, 1791 (1989).
[34] S. Glasstone, K. J. Laidler, and H. Eyring, *The Theory of Rate Processes* (McGraw-Hill, New York, 1941).
[35] R. Busch, E. Bakke, and W. L. Johnson, Acta Mater. **46**, 4725 (1998).
[36] Y. Q. Cheng, H. W. Sheng, and E. Ma, Phys. Rev. B **78**, 014207 (2008).